AD-A172 811 INVESTIGATION OF INTERACTIVE STRUCTURAL AND CONTROLLER SYNTHESIS FOR LARG..(U) MCINTOSH STRUCTURES DYNAMICS INC PALO ALTO CA* S C MCINTOSH ET AL. 22 JAN 86 TR-86-1 AFOSR-TR-86-0900 F49620-84-C-0025 F/G 22/2 1/1 NL

UNCLASSIFIED

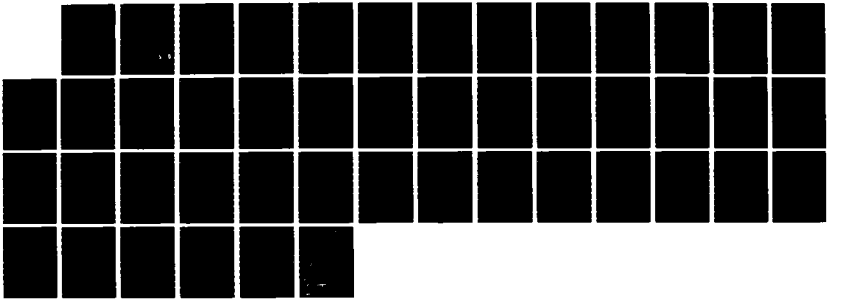

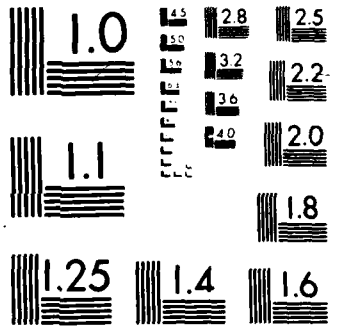
1.0
1.1
1.25
1.4
1.6
1.8
2.0
2.2
2.5
2.8
3.2
3.6
4.0
4.5
5.0

INVESTIGATION OF INTERACTIVE STRUCTURAL AND CONTROLLER SYNTHESIS FOR LARGE SPACECRAFT

Technical Report 86-1

January 22, 1986

PREPARED BY:

Samuel C. McIntosh, Jr.
McIntosh Structural Dynamics, Inc.

and

Michel A. Floyd
Integrated Systems, Inc.

PREPARED FOR:

Air Force Office of Scientific Research
Bolling Air Force Base, DC

McIntosh Structural Dynamics, Inc.
887 Warren Way
Palo Alto, CA 94307

Unclassified

SECURITY CLASSIFICATION OF THIS PAGE

AD-A173 811

REPORT DOCUMENTATION PAGE

1a REPORT SECURITY CLASSIFICATION: Unclassified	1b RESTRICTIVE MARKINGS
2a SECURITY CLASSIFICATION AUTHORITY	3 DISTRIBUTION/AVAILABILITY OF REPORT: Approved for public release; distribution unlimited.
2b DECLASSIFICATION/DOWNGRADING SCHEDULE	
4 PERFORMING ORGANIZATION REPORT NUMBER(S): Technical Report 86-1	5 MONITORING ORGANIZATION REPORT NUMBER(S): AFOSR-TR- 86-0900
6a NAME OF PERFORMING ORGANIZATION: McIntosh Structural Dynamics, Inc. / 6b OFFICE SYMBOL (If applicable)	7a NAME OF MONITORING ORGANIZATION: Air Force Office of Scientific Research
6c ADDRESS (City, State and ZIP Code): 887 Warren Way, Palo Alto, CA 94303	7b ADDRESS (City, State and ZIP Code): Building 410, Bolling AFB, DC 20332
8a NAME OF FUNDING/SPONSORING ORGANIZATION: AFOSR / 8b OFFICE SYMBOL (If applicable): NA	9 PROCUREMENT INSTRUMENT IDENTIFICATION NUMBER: F49620-84-C-0025
8c ADDRESS (City, State and ZIP Code): Bolling AFB DC 20332-6448	10 SOURCE OF FUNDING NOS. — PROGRAM ELEMENT NO.: 61102F / PROJECT NO.: 2302 / TASK NO: B1 / WORK UNIT NO.
11 TITLE (Include Security Classification): See back of page	

12 PERSONAL AUTHOR(S): McIntosh, Samuel C., Jr.; Floyd, Michel A., Integrated Systems, Inc.

13a TYPE OF REPORT	13b TIME COVERED	14 DATE OF REPORT (Yr., Mo., Day)	15 PAGE COUNT
Final Report	FROM 84MAR01 TO 85OCT30	86JAN22	44

16 SUPPLEMENTARY NOTATION

17 COSATI CODES			18 SUBJECT TERMS (Continue on reverse if necessary and identify by block number)
FIELD	GROUP	SUB. GR.	
	29	.11	

19 ABSTRACT (Continue on reverse if necessary and identify by block number)

A technique is developed for least-weight optimal design of a tubular-truss space structure, subject to constraints on its natural frequencies and its open-loop disturbance-rejection properties. The disturbance-rejection properties of the structure are measured by disturbance-to-regulated-variable grammians. It is shown how this technique can be embedded in a model-reduction scheme based on internal balancing. Examples treated include a simple "dumbbell" model and CSDL Model No. 1.

20 DISTRIBUTION/AVAILABILITY OF ABSTRACT	21 ABSTRACT SECURITY CLASSIFICATION	
UNCLASSIFIED UNLIMITED ☒ SAME AS RPT ☐ DTIC USERS ☐	Unclassified	
22a NAME OF RESPONSIBLE INDIVIDUAL: Dr. A.K. Amos	22b TELEPHONE NUMBER (Include Area Code): (202) 767-4937	22c OFFICE SYMBOL: AFOSR/NA

DD FORM 1473, 83 APR — EDITION OF 1 JAN 73 IS OBSOLETE

Unclassified

SECURITY CLASSIFICATION OF THIS PAGE

UNCLASSIFIED

Block #11: 'Investigation of Interactive Structural and Controller Synthesis for Large Spacecraft"

FOREWORD

This is the final report for contract F49620-84-C-0025, entitled "Development of Techniques for Interactive Structural and Controller Synthesis for Control-Configured Spacecraft", from the Air Force Office of Scientific Research. The Program Manager was Dr. A.K. Amos. Integrated Systems, Inc. was a subcontractor. The period of work covered by this report is March 1, 1984 through October 30, 1985.

TABLE OF CONTENTS

SECTION 1

PROBLEM DESCRIPTION

Large, flexible spacecraft have ambitious performance requirements that must be met in the presence of a variety of disturbances. The natural-frequency spectrum of such spacecraft is typically quite dense, with a number of modes below 1.0 Hz, and damping levels are small. Active controls, whether for maneuvering or for disturbance rejection, interact strongly with the flexible structural modes. The design of controllers for these spacecraft involves such problems as the selection of a reduced-order structural model, the choice of sensor and actuator types and locations, and the control strategy itself. Traditionally, this has been preceded by the design of the structure, with very little interaction between the two processes, as is illustrated in Figure 1. In view of the advances that have been made separately in the optimal design of structures and controls, great interest has arisen in integrating the two into a single optimal design problem.

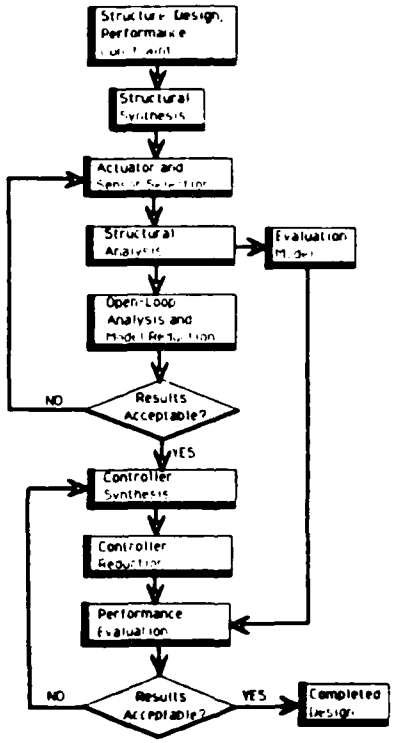

Figure 1. Serial Structural and Controller Synthesis Procedure for Large Spacecraft.

The controllers considered fall naturally into two classes: those for maneuver control and those for vibration regulation. References 1 and 2 are recent examples of work with the former type. The integrated problem involves solving for both structural parameters and an optimal control for a specified maneuver. Both References 1 and 2 use modal truncation in order to reduce the size of the problem.

Approaches to integrated design for vibration regulation have for the most part considered a system with a linear regulator. The model is not reduced, and the cost function involves both structural parameters and the elements of a feedback gain matrix. In References 3 and 4, the gains are determined so as to minimize a quadratic cost function that is combined with a structural cost function. Reference 5 has a more general formulation, in that the gains are controlled by eigenvalue placement, and more freedom is allowed in selecting the cost function. More specialized approaches include those of References 6 and 7. In Reference 6, lattice plate finite elements based on a continuum model of a large space structure are used; these elements permit an evaluation of the effects of structural parameter variations on the performance of reduced-order linear quadratic regulators. In Reference 7, an algorithm to obtain maximal reduction in required control strength for a minimal structural modification is developed and demonstrated for a colocated force-actuator velocity-sensor pair. A completely different approach to integrated design with set-theoretic methods is proposed in Reference 8.

With the exception of References 1, 2, and 6, where model-reduction schemes are employed, none of the work cited above deals with one of the principal problems that arises in the design of controllers for truly large spacecraft - the need to adopt a lower-order model both for evaluation purposes and for implementing a practical controller. This is understandable, since the simultaneous design of a structure and a full-order controller is conceptually an enormous task for large systems, without the added complication of including an estimator for a lower-order controller. Furthermore, the model-reduction task itself is far from simple, and there are many different schemes for accomplishing it.

Consider now the generic problem of reducing the effects of disturbances so as to achieve a desired level of performance in a large, flexible spacecraft. Clearly, the role of the controller is to augment whatever disturbance-rejection qualities the spacecraft structure may inherently exhibit. This implies that the controller must be effective where the structure is least effective. And, once the reduced-order model has been selected, filtering is one of the principal steps taken to avoid problems from spillover effects. These considerations lead to exploring the use of automated structural redesign for two purposes:

(1) To enhance as much as possible the inherent disturbance-rejection qualities of the structure, and

(2) To shape the frequency spectrum, if needed, in order to provide adequate spacing for frequency isolation of the controller.

As will be seen, some control over the frequency spectrum is helpful in any event.

This is the controller/structure interaction problem that is considered in this report. Since the structural redesign takes place before the loop is closed, this is not a truly integrated approach. It is, however, a necessary first step in the development of an integrated design capability for realistic large-scale structures. Moreover, it will be shown that the techniques developed here are readily extendable to the integrated structure/controller design problem.

SECTION 2
TECHNICAL APPROACH

2.1 Model Reduction

The framework for the approach to structural redesign is provided by a model-reduction scheme based on internal balancing (Reference 9).

A linear, time-invariant, asymptotically stable system has equations of motion that can be written in the familiar form

$$\begin{aligned} \{\dot{x}\} &= [A]\{x\} + [B]\{u\} \\ \{y\} &= [C]\{x\} \end{aligned} \tag{1}$$

Here $\{x\}$ is a column of system states, $[A]$ is the system matrix, $\{u\}$ is a column of control inputs, $[B]$ is the control distribution matrix, $\{y\}$ is a column of outputs, $[C]$ is the corresponding distribution matrix, and the dot symbol $(\cdot)$ denotes differentiation with respect to time t. The controllability grammian $[W_C]^2$ and observability grammian $[W_O]^2$ are given by

$$\begin{aligned} [W_C]^2 &= \int_O^\infty e^{[A]t}[B][B]^T e^{[A]^T t} dt \\ [W_O]^2 &= \int_0^\infty e^{[A]^T t}[C]^T[C] e^{[A]t} dt \end{aligned} \tag{2}$$

The system represented by Equation 1 is said to be internally balanced if

$$[W_C]^2 = [W_O]^2 = [\textstyle\sum]^2, \tag{3}$$

where the elements of the diagonal matrix $[\sum]$ are $\sigma_1^2, \sigma_2^2, \ldots, \sigma_n^2$, with n being the order of the system, and $i < j$ implying $\sigma_i^2 \leq \sigma_j^2$. It is shown in Reference 9 that any model of the form (1) can be taken to internally balanced form by a similarity transformation on the states $\{x\}$. It is also shown that if a balanced model is partitioned into, say, two subsystems, then the subsystems are also asymptotically stable (special steps must be taken if the σ_i^2 are not distinct).

The ability to quantify controllability and observability rankings and the stability property of subsystems are attractive characteristics for a model-reduction scheme. However, the need for similarity transformation and the concomitant loss of the original model states is undesirable, particularly for large-scale systems. This undesirable effect can be avoided if the structure is lightly damped and has decoupled dynamics; one is therefore led naturally to a modal state-space representation of a large-spacecraft structural-dynamics model in the form

$$\begin{Bmatrix} \dot{\eta}_1 \\ \dot{\eta}_i \end{Bmatrix} = \begin{bmatrix} -2\zeta_i\omega_i & -\omega_i^2 \\ 1 & 0 \end{bmatrix} \begin{Bmatrix} \dot{\eta}_i \\ \eta_i \end{Bmatrix} + \begin{bmatrix} b_i \\ 0 \end{bmatrix} \{u\} + \begin{bmatrix} d_i \\ 0 \end{bmatrix} \{w\}, i = 1, 2, \ldots, n$$

$$\{z\} = \sum_{i=1}^{n} [m_{1_i}\ m_{2_i}] \begin{Bmatrix} \dot{\eta}_i \\ \eta_i \end{Bmatrix} \tag{4}$$

$$\{y\} = \sum_{i=1}^{n} [c_{1_i}\ c_{2_i}] \begin{Bmatrix} \dot{\eta}_i \\ \eta_i \end{Bmatrix}$$

There are n modal coordinates η_i, with frequency ω_i and damping ratio ζ_i. The i^{th} row of $[B]$ is $[b_i]$, and the i^{th} row of the distribution matrix $[D]$ is $[d_i]$. The disturbance inputs are $\{w\}$ and the measurements are $\{z\}$. The measurement matrix $[M]$ and regulated-variable matrix $[C]$ are partitioned into blocks multiplying $\{\dot{\eta}_i\}$ and $\{\eta_i\}$, and the i^{th} columns of these blocks are denoted by $\{m_{1_i}\}, \{m_{2_i}\}, \{c_{1_i}\}$, and $\{c_{2_i}\}$, respectively. The performance measure for the controller is assumed to be

$$J = \lim_{t \to \infty} E(\{y\}^T \{y\}) \tag{5}$$

Let this model be the evaluation model (see Figure 1). In Reference 9 it is shown that the internal-balancing transformation simplifies, for $\zeta_i \ll 1$ and certain conditions on the frequency separation, to a simple diagonal scaling transformation. The modal decoupling is thus preserved in the internally balanced form of the model, and in fact it is not necessary to deal explicitly with the transformed model. The elements of the (equal) controllability and observability grammians are given by

$$\sigma_i^2 = \frac{1}{4\zeta_i\omega_i} \left([b_i][b_i]^T \left(\{c_{1_i}\}^T \{c_{1_i}\} + \frac{1}{\omega_i^2} \{c_{2_i}\}^T \{c_{2_i}\} \right) \right)^{\frac{1}{2}} \tag{6}$$

The actual modal-selection process of Reference 9 applies the internal-balancing concept to four separate input-output pairs:

- Disturbability to regulated variable: $[\sum]_{DC}^2$
- Controllability to regulated variable: $[\sum]_{BC}^2$
- Disturbability to sensors: $[\sum]_{DM}^2$
- Controllability to sensors: $[\sum]_{BM}^2$

The subscripts correspond to the various matrices that are involved in the computations of the grammians. Thus the second grammian, $[\sum]_{BC}^2$, corresponds to the example given above. The elements of these grammians will be identified with the same subscripts, and expressions for all of these resemble the expression (6) above for $\sigma_{BC_i}^2$.

The elements of $[\sum]^2_{DC}$ give modal rankings based on open-loop performance. Large values indicate relatively large disturbance propagation to the output. These measures are similar, but not equivalent, to the modal costs of Reference 10.

The elements of $[\sum]^2_{BC}$ permit rankings based on the modal controllability of the performance. A small value of the i^{th} element indicates that the given actuator configuration cannot directly affect the contribution of the i^{th} mode to the performance.

The elements of $[\sum]^2_{DM}$ rank the observability of disturbances in the sensors. A mode whose corresponding element in this matrix is relatively small may be difficult to estimate on-line.

The elements of $[\sum]^2_{BM}$ provide a mode-by-mode measure of potential controller authority for the given set of actuators and sensors.

The mode-selection process involving these four rankings is summarized as follows (Reference 9):

1. Select the modes having the largest $\sigma^2_{DC_i}$. These modes contribute most to the performance objectives, and with reasonable actuator and sensor placements, it should be possible to control each of the modes to some extent.

2. Examine the $\sigma^2_{BM_i}$. Include in the design model any highly controllable/measurable modes not selected in Step 1, especially if they are close in frequency to selected modes. Omission of these modes can cause spillover, which can destabilize the system.

3. Examine the $\sigma^2_{DM_i}$ and the $\sigma^2_{BC_i}$. Unselected modes having large values in either of these rankings indicate actuator/sensor configuration pathologies. A large $\sigma^2_{DM_i}$ indicates an unmodelled mode in the measurements, which will inhibit state estimation. An unmodelled mode with large $\sigma^2_{BC_i}$ may be driven in unpredictable ways by the controller to the detriment of performance. In either case, the modes should be included.

2.2 Structural Redesign

As is indicated in the foregoing discussion, the process of model reduction can be complicated, and combining it *ab initio* with an automated structural redesign procedure is not warranted. A more useful first step is to consider the open-loop problem and deal solely with the effects of disturbances on the performance as measured by the $\sigma^2_{DC_i}$. It is also useful to exert some control over the frequency spectrum. These considerations lead to the following problem statement:

Minimize $W(t_i), i = 1, 2, \ldots, N_d$

subject to

$$\begin{aligned} \sigma^2_{DC_i} &\leq \bar{\sigma}_i, \quad i = 1, 2, \ldots, N_g \\ \underline{\omega}_i \leq \omega_i &\leq \bar{\omega}_i, \quad i = 1, 2, \ldots, N_f \\ \underline{t}_i \leq t_i &\leq \bar{t}_i, \quad i = 1, 2, \ldots, N_d \end{aligned} \tag{7}$$

The objective function is the weight W, parameterized as a function of N_d design variables t_i. The behavioral constraints are represented by upper bounds $\bar{\sigma}_i$ on N_g grammians $\sigma^2_{DC_i}$, and upper bounds $\bar{\omega}_i$ and lower bounds $\underline{\omega}_i$ on the frequencies ω_i of N_f modes. Side constraints $\underline{t}_i$ and $\bar{t}_i$ can be imposed on the design variables. The scenario envisaged here is one in which a designer is seeking to improve a design judged deficient in its disturbance-rejection capabilities, as measured by the $\sigma^2_{DC_i}$, while at the same time tailoring the structure's natural-frequency spectrum to improve filtering or to avoid frequency excursions into an undesirable band. Making weight the objective serves to ensure, at the least, a minimum weight addition to achieve the desired behavior, and the designer can trade off weight against structural capabilities by varying the constraint bounds. This scenario is illustrated in Figure 2.

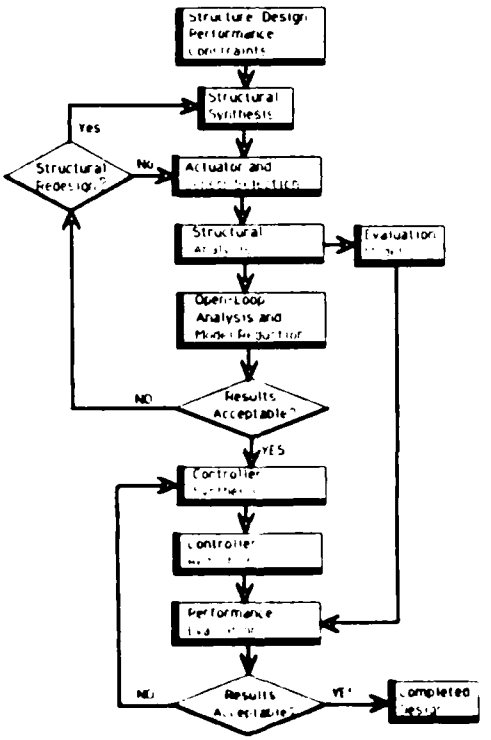

Figure 2. Initial Interactive Structural and Controller Synthesis Procedure for Large Spacecraft.

As posed above, this structural redesign problem is amenable to solution by a number of optimal search techniques. Virtually all of these techniques require sensitivity information in the form of derivatives of the objective and constraints with respect to

the design variables. While these derivatives can be obtained by finite differencing, it is generally more efficient to compute them from analytical expressions.

First, it is necessary to parameterize the structure itself. The structure is modeled with finite elements, and nodal locations are assumed fixed (i.e., shape changes are excluded). Design variables are typically member sizes, such as bar cross-sectional areas or plate thicknesses. Since space structures are very commonly made up from trusses, the elements to be used are restricted to tubular bar elements. For a thin-walled tubular cross section of radius R and thickness d, the inertial and stiffness properties vary as shown in Table 1. Three resizing options are permitted:

(1) Vary only the tube thickness, with side constraints to ensure that the thin-wall assumption is not violated.

(2) Vary only the radius; side constraints are also applicable here to preserve the thin-wall assumption.

(3) Scale the complete cross section - i.e., both the radius and thickness vary in the same proportion.

TABLE 1.

Variation of Inertial and Stiffness Properties of a Thin-Walled Tubular Cross Section of Radius R and Thickness d.

	Axial	Bending	Torsion
Inertial	Rd	Rd	R^3d
Stiffness	Rd	R^3d	R^3d

For any combination of these options, the discrete mass and stiffness matrices of the structure can be parameterized as follows:

$$[K] = [K_o] + \sum_{i=1}^{Nd} (t_i)^{h_i} [K_i]$$
$$[M] = [M_o] + \sum_{i=1}^{Nd} (t_i)^{k_i} [M_i] \tag{8}$$

The matrices $[K_o]$ and $[M_o]$ represent nonactive structure, or structure that is not to be resized (payload, for example). Note that once the geometry of the structure is fixed, the matrices $[K_o], [K_i], [M_o]$, and $[M_i]$ are fixed. Therefore computation of derivatives, as well as updating the mass and stiffness matrices, is particularly simple.

In a manner consistent with Equation (9), the weight can be expanded as

$$W = W_o + \sum_{i=1}^{Nd} (t_i)^{m_i} W_i \tag{9}$$

If the tube's thickness or its radius is the design variable, then $m = 1$. For the scaling of the complete cross section, $m = 2$.

To transform to modal coordinates, the system eigenvector matrix $[\phi]$ is needed. At this point, another important assumption is made. In order to reduce the size of the analysis problem during redesign, the eigenvectors of the initial design are used as basis vectors for the transformation to modal coordinates during the redesign process. Thus the order of the model during redesign remains that of the evaluation model, rather than that of the original discrete model. (Some accuracy may possibly be sacrificed, particularly if the design changes significantly. However, if accuracy is unduly compromised, $[\phi]$ can easily be updated.) With $[GK] = [\phi]^T[K][\phi], [GM] = [\phi]^T[M][\phi]$, Equations (8) transform to

$$\begin{aligned} [GK] &= [GK_o] + \sum_{i=1}^{Nd} (t_i)^{k_i} [GK_i] \\ [GM] &= [GM_o] + \sum_{i=1}^{Nd} (t_i)^{k_i} [GM_i] \end{aligned} \tag{10}$$

The modal coordinates $\{\eta\}$ from Equation (4) are related to the discrete coordinates $\{q\}$ as

$$\{q\} = [\phi][\psi]\{\eta\} \tag{11}$$

Here $[\psi]$ is a square eigenvector matrix in modal coordinates that must be updated at each redesign step. The disturbance-to-regulated-variable grammian $\sigma^2_{DC_i}$ is

$$\sigma^2_{DC_i} = \frac{1}{4\zeta_i\omega_i} \left([d_i][d_i]^T \left(\{c_{1_i}\}^T\{c_{1_i}\} + \frac{1}{\omega_i^2}\{c_{2_i}\}^T\{c_{2_i}\} \right) \right) \tag{12}$$

The discrete regulated-variable distribution matrix $[\bar{C}]$ and disturbance distribution matrix $[\bar{D}]$ are related to their modal counterparts through the transformation (11):

$$\begin{aligned} [C] &= \begin{bmatrix} C_1 & \\ & C_2 \end{bmatrix} = [\bar{C}] \begin{bmatrix} [\phi][\psi] & \\ & [\phi][\psi] \end{bmatrix} \\ [D] &= [\psi]^T[\phi]^T[\bar{D}] \end{aligned} \tag{13}$$

Hence

$$\begin{aligned} [d_i] &= \{\psi_i\}^T[\phi]^T[\bar{D}] \\ \{c_{1_i}\} &= [\bar{C}_1][\phi]\{\psi_i\} \\ \{c_{2_i}\} &= [\bar{C}_2][\phi]\{\psi_i\} \end{aligned} \tag{14}$$

where $\{\psi_i\}$ is the ith column of $[\psi]$. The problem of computing $\partial\sigma^2_{DC_i}/\partial t_i$ therefore reduces to that of computing the derivatives of $\{\psi_i\}$ and ω_i. The undamped modal representation of the system is given by

$$\Big([GK] - \omega_i^2[GM]\Big)\{\psi_i\} = \{0\} \tag{15}$$

Differentiating this equation with respect to t_j yields

$$\Big([GK_{,j}] - \omega_i^2[GM_{,j}] - 2\omega_i\frac{\partial\omega_i}{\partial t_j}[GM]\Big)\{\psi_i\} + \Big([GK] - \omega_i^2[GM]\Big)\{\psi_{i,j}\} = \{0\} \tag{16}$$

where $[GK_{,j}] = [\frac{\partial GK}{\partial t_j}]$, etc.

Pre-multiplying Equation (15) by $\{\psi_i\}^T$ and solving for $\partial\omega_i/\partial t_i$ gives (Reference 11)

$$\frac{\partial\omega_i}{\partial t_j} = \frac{\{\psi_i\}^T\Big([GK_{,j}] - \omega_i^2[GM_{,j}]\Big)\{\psi_i\}}{2\omega_i\{\psi_i\}^T[GM]\{\psi_i\}} \tag{17}$$

This is a very simple expression that is useful if only $\partial\omega_i/\partial t_j$ is needed. To get the eigenvector derivative, it is preferable to add a normalization condition and solve for the eigenvector and eigenvalue derivatives simultaneously (Reference 12). Let

$$\{\psi_i\}^T[GM]\{\psi_i\} = 1, \tag{18}$$

so that

$$2\{\psi_i\}^T[GM]\{\psi_{i,j}\} = -\{\psi_i\}^T[GM_{,j}]\{\psi_i\} \tag{19}$$

Combining Equations (16) and (19) produces the linear system

$$\begin{bmatrix} [GK] - \omega_i^2[GM] & -2\omega_i[GM]\{\psi_i\} \\ 2\{\psi_i\}^T[GM] & 0 \end{bmatrix}\begin{Bmatrix} \frac{\partial\psi_i}{\partial t_j} \\ \frac{\partial\omega_i}{\partial t_j} \end{Bmatrix} = -\begin{Bmatrix} \Big([GK_{,j}] - \omega_i^2[GM_{,j}]\Big)\{\psi_i\} \\ \{\psi_i\}^T[GM_{,j}]\{\psi_i\} \end{Bmatrix} \tag{20}$$

From Equations (10),

$$\begin{aligned}[GK_{,j}] &= h_j(t_j)^{h_j-1}[GK_j] \\ [GM_{,j}] &= k_j(t_j)^{k_j-1}[GM_j]\end{aligned} \tag{21}$$

Equation (12) can be simplified somewhat by making use of Equation (14). The products in Equation (12) become

$$\begin{aligned}\delta_i = [d_i][d_i]^T &= \{\psi_i\}^T[\phi]^T[\bar{D}][\bar{D}]^T[\phi]\{\psi_i\} \\ &= \{\psi_i\}^T[G\bar{D}]\{\psi_i\} \\ \sigma_{1_i} = \{c_{1_i}\}^T\{c_{1_i}\} &= \{\psi_i\}^T[\phi]^T[\bar{C}_1]^T[\bar{c}_1][\phi]\{\psi_i\} = \{\psi_i\}^T[G\bar{C}_1]\{\psi_i\} \\ \sigma_{2_i} = \{c_{2_i}\}^T\{c_{2_i}\} &= \{\psi_i\}^T[G\bar{C}_2]\{\psi_i\}\end{aligned} \tag{22}$$

Like the matrices $[GK_i]$ and $[GM_i]$, the matrices $[G\bar{D}]$, $[G\bar{C}_1]$, and $[G\bar{C}_2]$ are invariant during re-design. They are also symmetric, so that

$$\begin{aligned}\frac{\partial\delta_i}{\partial t_j} &= 2\{\psi_i\}^T[G\bar{D}]\{\psi_{i,j}\} \\ \frac{\partial\sigma_{1i}}{\partial t_j} &= 2\{\psi_i\}^T[G\bar{C}_1]\{\psi_{i,j}\} \\ \frac{\partial\sigma_{2i}}{\partial t_j} &= 2\{\psi_i\}^T[G\bar{C}_2]\{\psi_{i,j}\}\end{aligned} \tag{23}$$

Chain-rule differentiation of Equation (12) produces the desired derivative of $\sigma^2_{DC_i}$:

$$\frac{\partial\sigma^2_{DC_i}}{\partial t_j} = \frac{\partial\sigma^2_{DC_i}}{\partial\omega_i}\frac{\partial\omega_i}{\partial t_j} + \frac{\partial\sigma^2_{DC_i}}{\partial\delta_i}\frac{\partial\delta_i}{\partial t_j} + \frac{\partial\sigma^2_{DC_i}}{\partial\sigma_{1_i}}\frac{\partial\sigma_{1i}}{\partial t_j} + \frac{\partial\sigma^2_{DC_i}}{\partial\sigma_{2i}}\frac{\partial\sigma_{2i}}{\partial t_j} \tag{24}$$

2.3 Optimization Procedure

Before the actual optimization strategy is discussed, it is desirable to recast the problem statement of Equations (7) into a generic form. The behavioral constraints are rewritten in dimensionless form as follows:

$$\begin{aligned}&(\sigma^2_{DC_i}/\bar{\sigma}_i) - 1 \le 0, \quad i = 1,2,\ldots,N_g \\ &(\omega_i/\bar{\omega}_i) - 1 \le 0 \\ &1 - (\omega_i/\underline{\omega}_i) \le 0 \qquad (i = 1,2,\ldots,N_f)\end{aligned} \tag{25}$$

If necessary, the objective function as expressed in Equation (9) can also be scaled in order to avoid numerical difficulties. Similarly, it is useful to view the design variables t_i as scale factors on the actual physical parameters. Thus the initial design is always characterized by $t_i = 1.0$ for all i. The optimization problem becomes

Minimize

$$W(t_i), \quad i = 1, 2, \ldots, N_d$$

subject to

$$\begin{aligned} G_j(t_i) &\leq 0, \quad j = 1, 2, \ldots, N_g + N_f \\ \underline{t}_i &\leq t_i \leq \bar{t}_i, \quad i = 1, 2, \ldots, N_d \end{aligned} \tag{26}$$

Here the constraint functions G_j take the appropriate forms as given in Equations (25).

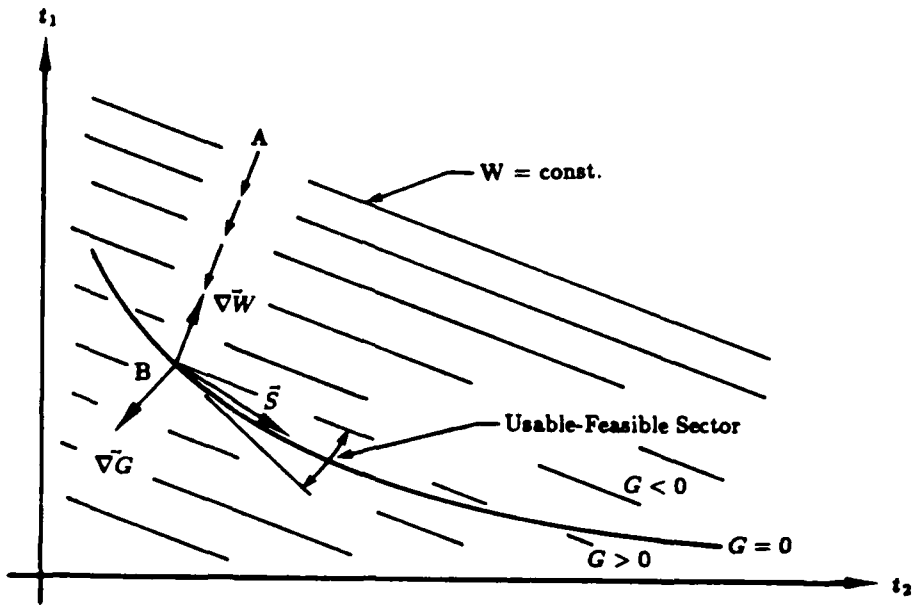

Figure 3. Direction-finding Problem at a Constraint Boundary.

The optimal search strategy is based on the method of feasible directions (Reference 13), as implemented in the general purpose optimization code CONMIN (Reference 14). The feasible-directions procedure is illustrated in Figure 3, for two design variables and a single constraint. If the initial design (A) is not at a constraint boundary, then the problem is at that point unconstrained, and a steepest-descent search direction is selected. This direction is followed until the constraint boundary is encountered (B). Let the search direction at point B be defined by the vector $\vec{S}$. The condition that this vector direction be feasible–that is, not violate the constraint within a linear approximation about B–is

$$\vec{S} \cdot \nabla \vec{G} \leq 0 \tag{27}$$

To be usable, this direction must also reduce the objective function. Within the same linear approximation, this requirement is expressed by

$$\vec{S} \cdot \nabla \vec{W} \leq 0 \tag{28}$$

These two conditions define the usable-feasible sector. Any design change within this sector will both reduce the objective function and satisfy the constraint.

CONMIN employs the method of Reference 13 to select $\vec{S}$. The direction vector and a scalar β are found such that β is maximized according to the following conditions:

$$\begin{aligned} \vec{S} \cdot \nabla \vec{G} + \theta\beta &\leq 0 \\ \vec{S} \cdot \nabla \vec{W} + \beta &\leq 0 \\ |\vec{S}| \quad &\text{bounded} \end{aligned} \tag{29}$$

Here β plays the role of a slack variable, which is added to the usable-feasible conditions and is scaled by a positive constant θ. When θ is unity, the feasible and usable conditions are equally biased. Other values of θ can be used to force the search dirction towards one sector boundary or the other. For example, if the constraint boundary is strongly concave, as in Figure 3, convergence would be enhanced by using a relatively high value of θ, which would force the search direction away from the constraint boundary.

Once $\vec{S}$ is selected, the search continues in that direction until a minimum in W is found or until the constraint boundary is again encountered. A new search direction is selected, and the process is continued until no improvement in W can be obtained.

The complete design process, from initial modeling through optimal redesign, is accomplished with a set of computer codes linked together as shown in Figure 4. In general, each code makes use of an input file and output files from codes previously run and creates a print output file and related files to be used by the next set of codes. The function of each code is discussed briefly below.

SAMGEN generates the mass and stiffness matrices for the system. SAMGEN also writes the matrices $[K_o], [K_i], [M_o]$, and $[M_i]$ to a file. These matrices are ordered according to design-variable information supplied by the user.

WEIGHT reads the SAMGEN input file and creates a file of the weight coefficients W_o and W_i.

DVLINK is a design-variable linking code. By linking design variables, any number of smaller design problems can be created from a single system model. DVLINK also scales the matrices associated with each design variable with user-supplied scale factors, so it is also possible to create any number of new designs from a single system model. If desired, the coefficients from WEIGHT can also be linked.

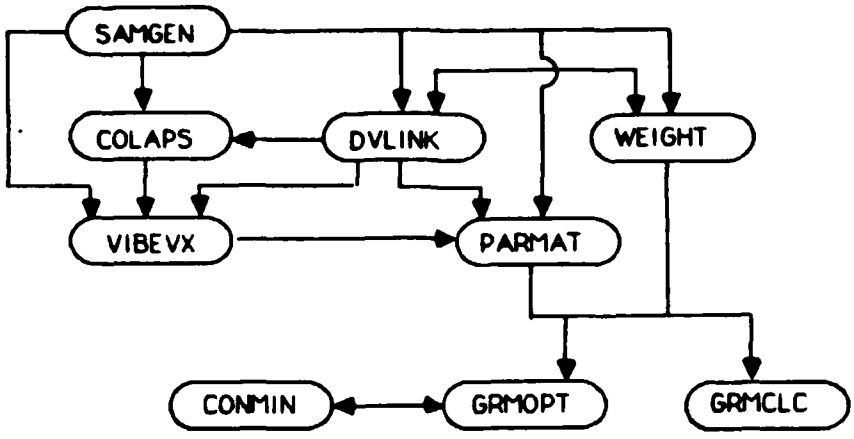

Figure 4. Flow of Information Among Codes.

COLAPS is a code that eliminates unwanted degrees of freedom from the system model by static reduction. Matrices from SAMGEN or DVLINK can be assembled and collapsed.

VIBEVX takes the collapsed mass and stiffness matrices or uncollapsed matrices from SAMGEN or DVLINK and computes the undamped frequencies and mode shapes.

PARMAT takes information from VIBEVX and SAMGEN or DVLINK and computes the generalized matrices $[GK_o], [GK_i], [GM_o], [GM_i], [G\bar{D}], [G\bar{C}_1]$, and $[G\bar{C}_2]$.

GRMOPT is the driver for CONMIN. All input, updating, and derivative calculations are performed in GRMOPT for designs determined by CONMIN.

GRMCLC is a version of GRMOPT that performs only the analysis and derivative calculations without calling CONMIN. It makes use of the same input file that GRMOPT does and is used to compute grammians and verify that the optimization problem is set up properly.

All the codes are written in Fortran and are run on DEC VAX-series computers under VMS.

2.4 Control Evaluation

The control engineer traditionally has little or no input into the design of the hardware he is supposed to control. This is true not only for large space structures, but also for most systems, including aircraft, spacecraft, automobiles, process control plants and

servos. In some cases, the control engineer may be able to specify the number, location, and site of sensors and actuators. The F-16 control-configured vehicle (CCV) is a rare example of control being integrated into the system engineering process from the very beginning.

Structural dynamics has only recently become of interest to spacecraft control engineers. Accustomed to relatively stiff structures and loose performance requirements, they have been able to deal with flexibility using sample design techniques. Now, driven by very stringent performance requirements, they have been forced to make use of all available tools and to come up with new ones. Unfortunately, the "large space structure" (LSS) control field has seen relatively little cooperation between the control and structures camps. Most control engineers try to solve the problem with purely active techniques, while most structures engineers, wary of things non-mechanical, prefer to use purely passive techniques. There are but a handful of engineers who have had formal training in both disciplines, especially when compared to the number who profess to be experts in both.

There is obviously much room for cooperation, which should make both the control and the structures engineers' jobs easier. Modal shaping and passive damping will improve robustness, and high–authority control will produce high performance without excessive structural mass. The control engineer thinks of a space structure as being "large" as soon as performance requirements force him to consider flexibility. Skylab was physically "large" but a space-based laser of comparable size represents a radically more difficult control problem.

In looking at structures from a control viewpoint, an LSS control engineer will typically look at this problem in the frequency domain. Given a closed-loop bandwidth dictated by performance requirements and disturbance spectra, the frequency scale may be divided into three regions (see Figure 5):

(1) The bandwidth - that part of the frequency scale where gain is high

(2) the crossover region, where the gain is rolling off, and

(3) the rest, where the controller has essentially no effect.

Structural modes inside the control bandwidth must normally be actively controlled, and those beyond the crossover region are usually ignored. The most difficult modes to deal with are those in the crossover region. Trying to control them actively simply increases the control bandwidth, moving the problem to a higher frequency. Yet these modes cannot be ignored because they can easily be driven unstable. A sharp roll-off or frequency shaping in the control system can help, but at the cost of decreasing robustness inside the control bandwidth (Figure 6).

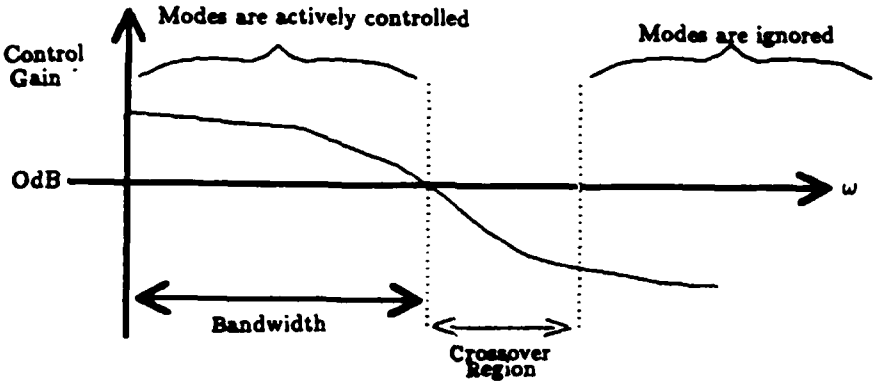

Figure 5. The Frequency Scale is Divided into Three Regions.

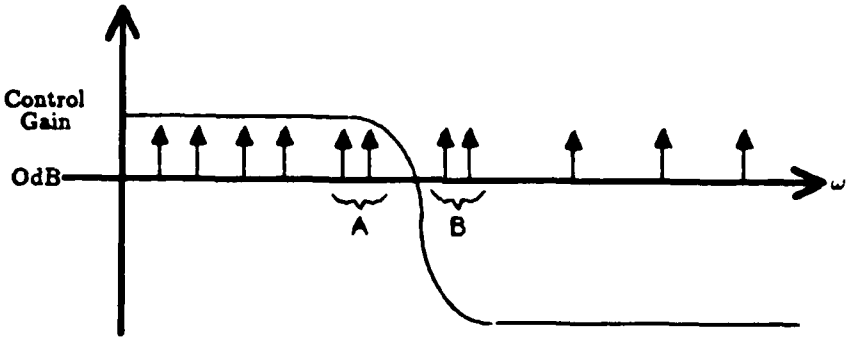

Figure 6. A Steep Roll-Off to Avoid Modes (B) May Cause Problems for Modes (A).

The ideal situation from the control engineer's viewpoint is to have a large natural gap in the structure's actual frequencies (Figure 7). Such a gap highlights the difference between modes that are clearly significant and those that can be ignored.

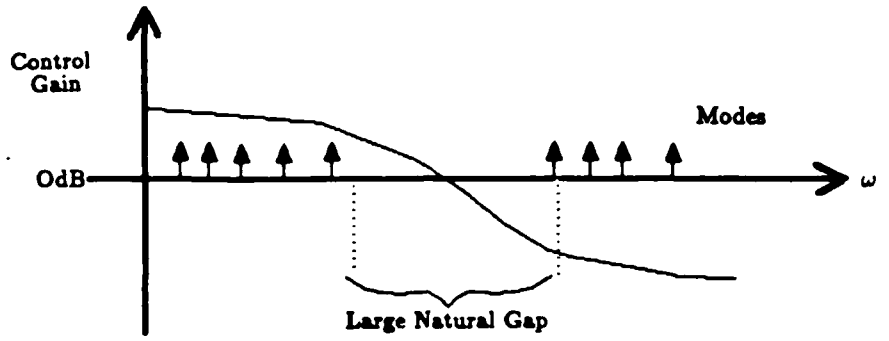

Figure 7. A Large Natural Frequency Gap Makes the Control Engineer's Job Easier.

Fortunately, frequency gaps occur quite naturally in many classes of structures. Structures with repeated elements exhibit strong modal clustering around the natural frequencies of the basic element (Figure 8). Although tight modal clustering can complicate the control engineer's task, the natural gaps help matters significantly. In complex structures with little symmetry and few repeated elements, clustering is reduced and there may be no identifiable gaps (Figure 9).

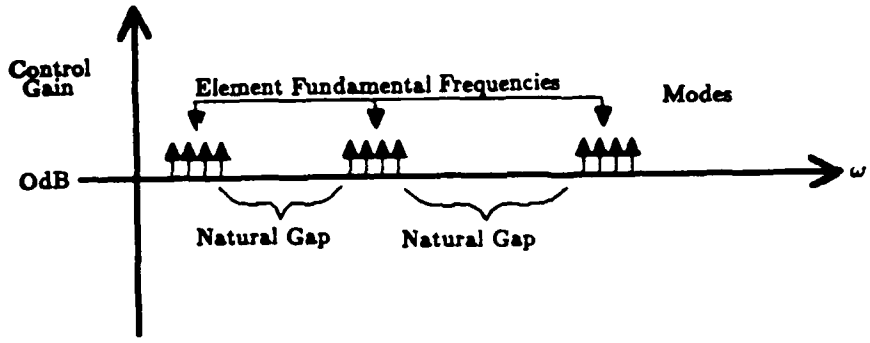

Figure 8. Natural Clustering in Repetitive and Symmetric Structures.

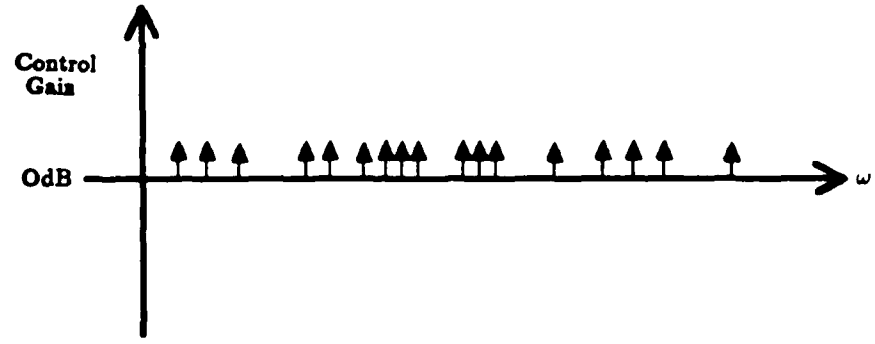

Figure 9. A "Control Nightmare".

The ability to shape the structure's frequency response characteristics can yield many other benefits to the control designer:

1. The structure's response to colored noise disturbances can be reduced by moving modes out of the frequency ranges of disturbances. Ideally, one would shape the transfer function to place transmission zeros over disturbances frequencies (this is essentially a structural notch filter). This would minimize the amount of effort that would have to be provided by the control system to reduce disturbances.

2. Modes that are closely spaced could be separated to make them more controllable, observable, and identifiable.

The control engineer's task can be thought of as creating a controller frequency response that, in combination with the structure's frequency response, yields desirable closed-loop time and frequency response.

SECTION 3
EXAMPLES

3.1 Dumbbell Model No. 1

The first system to be analyzed, a low-order beam model with point masses, is shown in Figure 10. Two five-foot aluminum tubes, with cross-section dimensions given in the figure, support a 10-lb mass at the center and 5-lb masses at each end. Free-free motion in the $y - z$ plane is allowed. The disturbances are a torque about the z axis and a load in the z direction at node 2, and the measurements combine the difference in z-direction displacements at nodes 1 and 3, and its rate.

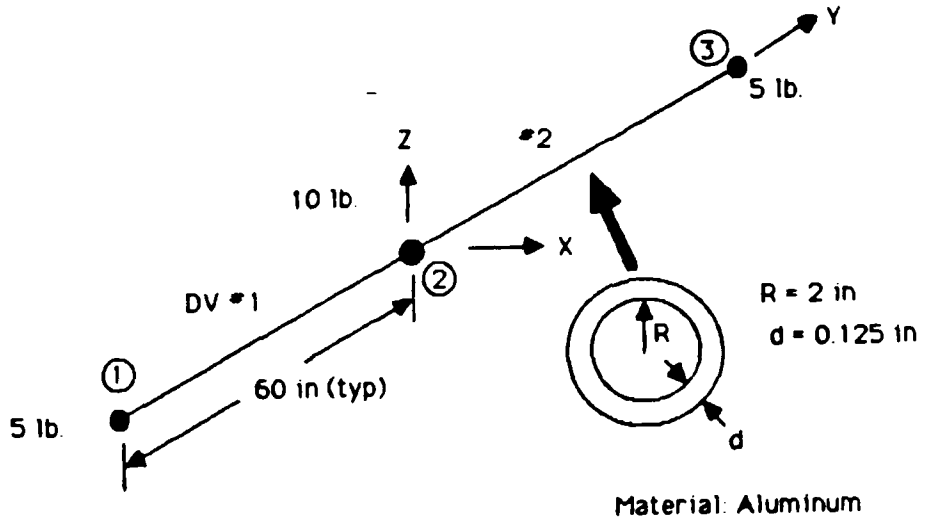

Figure 10. Layout of Dumbbell Model No. 1.

Table 2 gives the elastic frequencies computed for this model; there are also four rigid-body modes, corresponding to translations in the y and z directions and rotations about the x and y axes. Since the measurements are only affected by antisymmetric disturbances and modes, only the $\sigma^2_{DC_i}$ for antisymmetric modes involving z displacements are nonzero, and the torque disturbance is the only significant input. Modes 6 and 10 are the first two antisymmetric z bending modes, so these are the modes of interest here.

TABLE 2.

Elastic Natural Frequencies of Dumbbell Model No. 1.

Mode No.	5	6	7	8	9	10	11	12
Frequency, Hz	35.06	154.4	313.4	559.9	560.8	646.6	882.8	1120

Two design variables, representing scalings on cross-section properties for each beam segment, were allowed. The grammians for modes 6 and 10 were constrained, and lower frequency bounds were also imposed on these same modes. The four constraint functions thus took the following forms:

$$\begin{aligned} G_1 &= (\sigma^2_{DC_6}/0.310) - 1 \\ G_2 &= (\sigma^2_{DC_{10}}/0.130) - 1 \\ G_3 &= 1 - \omega_6/960.0 \\ G_4 &= 1 - \omega_{10}/4080 \end{aligned} \tag{29}$$

The frequencies are in rad/sec, and modal damping of 0.002 was assumed for the grammian calculations.

To validate the derivative calculations, finite-difference estimations were compared with analytical computations. GRMCLC was run for the initial design ($t_1 = t_2 = 1.0$) and then re-run with $t_2 = 1.02$ for each of the three resizing options. The results of this exercise are given in Tables 3-5. For the initial design, $\sigma^2_{DC_6} = 0.3086$, $\sigma^2_{DC_{10}} = 0.1197, \omega_6 = 970.0$ rad/sec, and $\omega_{10} = 4063$ rad/sec. The expected increase in sensitivity as t, R, and then R and d simultaneously are resized, is demonstrated. Much more striking is the near-perfect agreement between the finite-difference and the averaged analytical derivatives.

TABLE 3.

Comparison of Derivatives for Dumbbel Model No. 1, for Resizing Option 1 (Scaling d).

	Finite Difference	Initial Design	Analytical Average	Perturbed Design ($t_2 = 1.02$)
$\partial G_1/\partial t_2$	-0.144	-0.1688	-0.1443	-0.1198
$\partial G_2/\partial t_2$	-0.079	-0.08161	-0.07898	-0.07636
$\partial G_3/\partial t_2$	-0.049	-0.04872	-0.04914	-0.04957
$\partial G_4/\partial t_2$	0.0206	0.02026	0.02055	0.02084

TABLE 4.

Comparison of Derivatives for Dumbbell Model No. 1, for Resizing Option 2 (Scaling R).

	Finite Difference	Initial Design	Analytical Average	Perturbed Design ($t_2 = 1.02$)
$\partial G_1/\partial t_2$	-0.653	-0.6664	-0.6526	-0.6387
$\partial G_2/\partial t_2$	-0.548	-0.5420	-0.5482	-0.5544
$\partial G_3/\partial t_2$	-0.558	-0.5539	-0.5586	-0.5634
$\partial G_4/\partial t_2$	0.528	0.5181	0.5282	0.5384

TABLE 5.

Comparison of Derivatives for Dumbbell Model No. 1, for Resizing Option 3 (Scaling R and d).

	Finite Difference	Initial Design	Analytical Average	Perturbed Design ($t_2 = 1.02$)
$\partial G_1/\partial t_2$	-0.854	-0.8352	-0.8538	-0.8723
$\partial G_2/\partial t_2$	-0.642	-0.6236	-0.6410	-0.6583
$\partial G_3/\partial t_2$	-0.614	-0.6026	-0.6139	-0.6252
$\partial G_4/\partial t_2$	0.555	0.5384	0.5548	0.5713

Because of this model's symmetry, there is really only one independent design variable, so no optimal redesign was attempted.

3.2 Dumbbell Model No. 2

In order to provide a more reasonable model for resizing, a model of the dumbbell system with more elements was created, as illustrated in Figure 11. There are now three design variables, as indicated in the figure. The measurements and disturbances are unchanged from those assumed for Model No. 1.

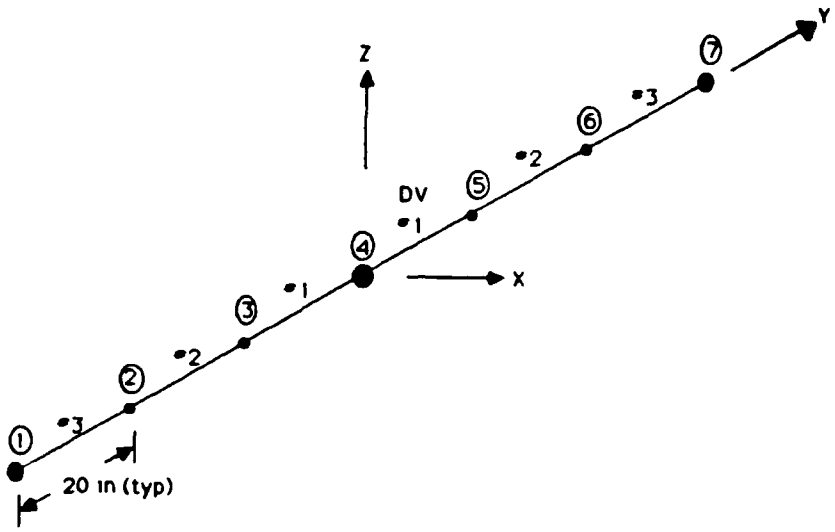

Figure 11. Layout of Dumbbell Model No. 2.

The elastic natural frequencies of this model are given in Table 6. This higher-order model has more modes that propagate the disturbance into the measurement; the three lowest-frequency modes are modes 6, 8, and 14. Modes 6 and 8 correspond to modes 6 and 10 in Model 1.

TABLE 6.

Elastic Natural Frequencies of Dumbbell Model No. 2.

Mode No.	5	6	7	8	9
Frequency, Hz	35.05	138.6	237.2	510.6	513.6
Mode No.	10	11	12	13	14
Frequency, Hz	553.2	680.0	880.2	1062	1235

To test the redesign procedure, an optimization problem was set up with this model of the dumbbell. The goal of this optimization problem was to reduce the grammian for mode 6 to 0.2200, with lower bounds on the frequencies up to mode 13 and an upper bound on the frequency of mode 8 as well. The results are summarized in Table 7. The optimized model is almost 4% heavier, and the active constraint is the upper bound on the grammian for mode 6. The design variables were constrained to be between 0.600 and 1.500; these limits were not encountered.

To assess the impact of using fixed mode shapes, normal modes were computed for the final design from Table 7, and the optimization procedure was restarted. These results

are given in Table 8. Comparison of the initial design of Table 8 with the final design of Table 7 gives an indication of the modeling error introduced as a result of fixing the mode shapes. The frequencies are in general slightly lower and the grammians slightly higher when the computations were done with normal modes. The final design variables in Table 8 indicate that the optimization process of Table 7 went slightly too far; the overall final design, given by the products of the final design values from the two tables, is given at the bottom of Table 8. In principle, one could continue this process by updating the modes again, but the results would not change significantly.

TABLE 7.

Results of Redesign of Dumbbell Model No. 2

Mode	Initial Frequency (rad/sec)	Design Constraint (rad/sec)	Initial Grammian $\sigma^2_{DC_i}$	Design Constraint (rad/sec)	Final Frequency (rad/sec)	Final Grammian $\sigma^2_{DC_i}$
5	220.2	$\geq$150.0			277.3	
6	870.8	$\geq$750.0	0.2652	$\leq$0.2200	815.2	0.2208
7	1490	$\geq$1200			1672	
8	3208	3210$\geq \omega \geq$2500	0.08655	$\leq$0.2200	3130	0.04579
9	3227	$\geq$3220			4008	
10	3476	$\geq$3220			4960	
11	4272	$\geq$3220			5436	
12	5530	$\geq$3220			5645	
13	6673	$\geq$3220			7265	
14	7760					

No. of Iterations 7

Initial Mass (lbs) 38.84

Final Mass (lbs) 40.28

Final Design Variables:

1.284 0.9655 0.8056

TABLE 8.

Redesign of Dumbbell Model No. 2 with Updated Normal Modes

Mode	Initial Frequency (rad/sec)	Design Constraint (rad/sec)	Initial Grammian $\sigma^2_{DC_i}$	Design Constraint (rad/sec)	Final Frequency (rad/sec)	Final Grammian $\sigma^2_{DC_i}$
5	268.1	$\geq$150.0			280.5	
6	790.6	$\geq$750.0	0.2325	$\leq$0.2200	850.2	0.2202
7	1629	$\geq$1200			1585	
8	3069	3210$\geq \omega \geq$2500	0.04579	$\leq$0.2200	3210	0.04596
9	3724	$\geq$3220			3796	
10	4281	$\geq$3220			4427	
11	4977	$\geq$3220			4845	
12	5213	$\geq$3220			5447	
13	6696	$\geq$3220			7308	
14	8000					

No. of Iterations 14

Initial Mass (lbs) 40.28

Final Mass (lbs) 40.65

Final Design Variables:

0.9559 1.084 1.028

Final Design Variables (Overall):

1.227 1.046 0.8280

3.3 CSDL Model No. 1

The next example is a generic model of a large-antenna feed horn, first proposed by the Charles Stark Draper Laboratory and known as CSDL Model No. 1. A layout of this model is shown in Figure 12; the data for this model were taken from Reference 15. The base of the horn is assumed fixed to ground; this is equivalent to neglecting any coupling between antenna motion and horn motion. The regulated quantity is the relative displacement (line-of-sight error, LOS) of node 1 in the $x-y$ plane, expressed as the x and y displacements of node 1; the disturbances are forces in all three coordinate directions at nodes 2, 3, and 4.

There are 12 design variables, one for each truss member in the structure. Because the nonactive inertia in this model is so much greater than the inertia in the truss members,

the nonactive inertia was not included in the weight calculation during the optimization, and the weight coefficients were scaled in order to avoid numerical problems.

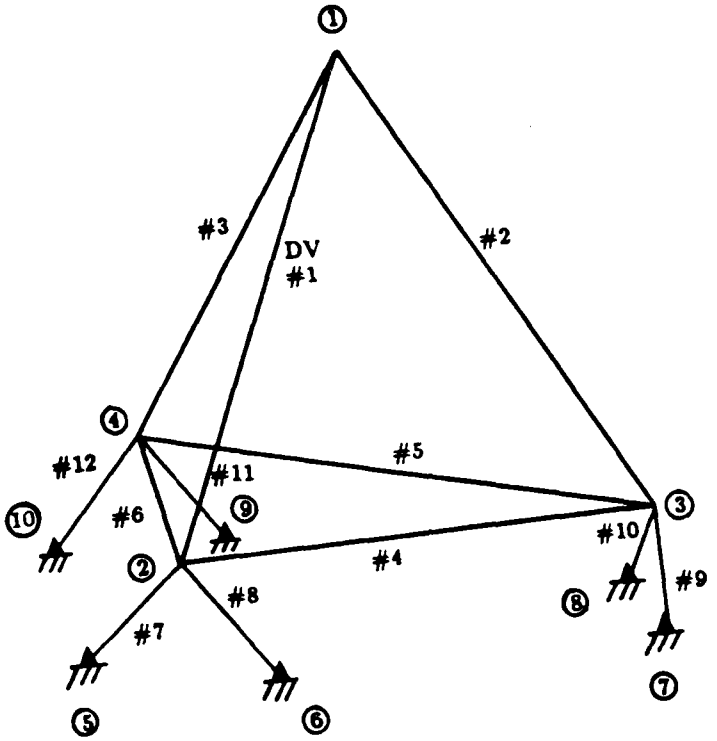

Figure 12. Layout of CSDL Model No. 1.

Frequencies and grammians for this model are given in Table 9. As can be seen, there are two groups of modes, for the most part isolated quite conveniently both spatially and temporally. Note that the grammians for modes 1 and 2 are much greater than those for the other modes.

TABLE 9.
Natural Frequencies and Grammians $\sigma^2_{DC_i}$ of CSDL Model No. 1.

Mode No.	Frequency, Hz	Grammian $\sigma^2_{DC_i}$
1	0.2152	166.1
2	0.2675	203.1
3	0.4701	19.47
4	0.4855	64.25
5	0.5493	59.77
6	0.6750	0.7488×10^{-4}
7	0.7487	6.536
8	0.7630	22.98
9	1.362	13.85
10	1.476	0.2267
11	1.640	8.907
12	2.057	2.220
13	40.88	0.1732×10^{-4}
14	44.86	0.1956×10^{-4}
15	52.63	0.3624×10^{-5}
16	55.52	0.5126×10^{-5}
17	55.79	0.2861×10^{-5}
18	73.31	0.2503×10^{-5}

A number of structural redesigns were run for the CSDL Model 1 structure. Results from four of these runs are shown here:

3.3.1 Run 1

The principal objective of this run was to decrease the grammians for modes 1 and 2. From Table 9, it can be seen that the first 12 modes, with the exception of mode 6, form the modal group that propagates the disturbances to the measurement. Hence, upper bounds of 100.0 were imposed on the grammians for this group. Lower bounds of 1.200 rad/sec were imposed on the frequencies in this group. To preserve the frequency separation between the 12th and 13th modes, an upper bound of 75.00 rad/sec was also applied to the frequency of mode 12, and a lower bound of 200.0 rad/sec was applied to the frequency of mode 13. Frequencies and grammians for the remaining modes were unconstrained. The design variables for this run were restricted to be between 0.800 and 1.500. Option 3 – that is, scaling the complete cross section – was selected for the sizing. Results for this run are shown in Table 10.

As can be seen from this table, the objectives were achieved with a reduction of around 31% in the structural weight. During the optimization, the active constraints were always a combination of the grammian constraints on modes 1 and 2, and the lower bound on the frequency of mode 1. This design was accomplished by reducing the members

forming the horn to, or very near to, their minimum allowable size while increasing the support members to near their maximum allowable size.

TABLE 10.

Results of Run 1 for CSDL Model 1.

Mode	Initial Frequency (rad/sec)	Design Constraint (rad/sec)	Initial Grammian $\sigma^2_{DC_i}$	Design Constraint	Final Frequency (rad/sec)	Final Grammian $\sigma^2_{DC_i}$
1	1.352	≥ 1.2	166.1	≤ 100	1.200	99.41
2	1.681	≥ 1.2	203.1	≤ 100	1.607	100.0
3	2.954	≥ 1.2	19.47	≤ 100	3.272	47.47
4	3.050	≥ 1.2	64.25	≤ 100	3.774	32.81
5	3.451	≥ 1.2	59.77	≤ 100	4.447	53.49
6	4.241	≥ 1.2	$.7488 \times 10^{-4}$	≤ 100	5.498	0.1575
7	4.704	≥ 1.2	6.536	≤ 100	6.051	6.112
8	4.794	≥ 1.2	22.98	≤ 100	6.325	0.2241
9	8.558	≥ 1.2	13.85	≤ 100	8.021	13.16
10	9.277	≥ 1.2	0.2267	≤ 100	8.444	0.5151
11	10.30	≥ 1.2	8.907	≤ 100	8.856	8.448
12	12.93	$1.2 \geq \omega \geq 75$	2.220	≤ 100	10.47	4.069
13	256.8	≥ 200	0.173×10^{-4}		286.5	

No. of Iterations 20

Initial Mass (Scaled) 5.24

Final Mass (Scaled) 3.61

Final Design Variables:

0.8 0.8 0.8332 0.8 0.8 0.8 1.376 1.374 1.229 1.487 1.488 1.232

3.3.2 Run 2

The objective of this run was essentially the same as that of Run 1, to reduce the grammians for modes 1 and 2 while retaining the desirable frequency separation between modes 12 and 13. However, all of the modes and grammians were constrained, and the frequency separation desired was increased to a full decade, from 20.00 to 200.0 rad/sec. Since the final design for Run 1 also meets these goals, the same final design was found here, although the optimization paths are different. The results for Run 2 are shown in Table 11.

TABLE 11.

Results of Run 2 for CSDL Model 1.

Mode	Initial Frequency (rad/sec)	Design Constraint (rad/sec)	Initial Grammian $\sigma^2_{DC_i}$	Design Constraint	Final Frequency (rad/sec)	Final Grammian $\sigma^2_{DC_i}$
1	1.352	≥ 1.2	166.1	≤ 100	1.200	99.41
2	1.681	≥ 1.2	203.1	≤ 100	1.607	100.00
3	2.954	≥ 1.2	19.47	≤ 100	3.272	47.47
4	3.050	≥ 1.2	64.25	≤ 100	3.774	32.81
5	3.451	≥ 1.2	59.77	≤ 100	4.447	53.49
6	4.241	≥ 1.2	$.7488 \times 10^{-4}$	≤ 100	5.498	0.1575
7	4.704	≥ 1.2	6.536	≤ 100	6.051	6.112
8	4.794	≥ 1.2	22.98	≤ 100	6.325	0.2241
9	8.558	≥ 1.2	13.85	≤ 100	8.021	13.16
10	9.277	≥ 1.2	0.2267	≤ 100	8.444	0.5151
11	10.30	≥ 1.2	8.907	≤ 100	8.856	8.448
12	12.93	$1.2 \geq \omega \geq 75$	2.220	≤ 100	10.47	4.069
13	256.8	≥ 200	0.173×10^{-4}		286.5	

No. of Iterations 20

Initial Mass (Scaled) 5.24

Final Mass (Scaled) 3.61

Final Design Variables:

0.8 0.8 0.8332 0.8 0.8 0.8 .376 1.374 1.229 1.487 1.488 1.232

3.3.3 Run 3

For this run, the grammian constraints on modes 9-18 were reduced to 10.00, and an attempt was made to introduce a frequency gap between modes 8 and 9 by imposing an upper bound of 10.00 rad/sec on the frequency of mode 8 and a lower bound of 20.00 rad/sec on the frequencies of modes 9-12. Hence the reduction of the grammians must be accompanied by a substantial increase in the frequencies of modes 9-12. As can be seen in Table 12, this could not be done within the confines of the bounds on the design variables. CONMIN quit after ten iterations failed to produce a feasible design. Not all of the design variables were at their upper limits, but it is clear that the grammian constraint on mode 2 and the lower frequency bounds on modes 9-12 could not be satisfied even if the structure were uniformly scaled by a factor of 1.5.

TABLE 12.

Results of Run 3 for CSDL Model 1.

Mode	Initial Frequency (rad/sec)	Design Constraint (rad/sec)	Original Grammian $\sigma^2_{DC_i}$	Design Constraint	Final Frequency (rad/sec)	Final Grammian $\sigma^2_{DC_i}$
1	1.352	≥ 1.2	166.1	≤ 100	1.655	78.45
2	1.681	≥ 1.2	203.1	≤ 100	2.412	117.30
3	2.954	≥ 1.2	19.47	≤ 100	4.346	18.50
4	3.050	≥ 1.2	64.25	≤ 100	4.709	34.61
5	3.451	≥ 1.2	59.77	≤ 100	5.275	41.69
6	4.241	≥ 1.2	$.7488 \times 10^{-4}$	≤ 100	6.430	0.3695×10^{-3}
7	4.704	≥ 1.2	6.536	≤ 100	6.767	6.201
8	4.794	$1.2 \geq \omega \geq 10$	22.98	≤ 100	7.198	13.29
9	8.558	≥ 20	13.85	≤ 10	12.85	9.388
10	9.277	≥ 20	0.2267	≤ 10	13.95	0.1054
11	10.30	≥ 20	8.907	≤ 10	15.49	5.900
12	12.93	≥ 20	2.220	≤ 10	19.41	1.465
13	256.8	≥ 20	0.173×10^{-4}	≤ 10	377.7	0.2682×10^{-4}
14	281.9	≥ 20	0.1956×10^{-4}	≤ 10		0.2861×10^{-4}
15	330.7	≥ 20	0.3624×10^{-5}	≤ 10		0.3576×10^{-5}
16	348.9	≥ 20	0.5126×10^{-5}	≤ 10		0.6556×10^{-5}
17	350.5	≥ 20	0.2861×10^{-5}	≤ 10		0.6556×10^{-5}
18	460.6	≥ 20	0.2503×10^{-5}	≤ 10		0.3576×10^{-5}

No. of Iterations 10

Initial Mass (Scaled) 5.24

Final Mass (Scaled) 11.65

Final Design Variables:

1.5 1.5 1.015 1.5 1.499 1.5 1.5 1.5 1.5 1.5 1.5 1.5

3.3.4 Run 4

For this run, an attempt was made to reduce the grammians for modes 1-5 to 50.00, and the design variables were allowed to move between limits of 0.500 and 2.000. All other constraints were the same as in Run 2. The results for this run are given in Table 13. The constraints were satisfied, but at the cost of an increase in structural weight of almost 30%. The active constraints were the grammians for modes 2,3, and 12. The design

strategy here was similar to that in Run 2, in that the horn member sizes were reduced and the support member sizes were increased. For this case, however, the upper-bound limits on the support-member sizes were encountered. Also, many more iterations were required. The constraints were satisfied after four iterations, with the structural weight almost doubled, and the remaining iterations were taken up with an agonizingly slow but ultimately successful effort to reduce this weight.

TABLE 13.

Results of Run 4 for CSDL Model 1.

Mode	Initial Frequency (rad/sec)	Design Constraint (rad/sec)	Initial Grammian $\sigma^2_{DC_i}$	Design Constraint	Final Frequency (rad/sec)	Final Grammian $\sigma^2_{DC_i}$
1	1.352	≥ 1.2	166.1	≤ 50	1.244	42.76
2	1.681	≥ 1.2	203.1	≤ 50	1.687	50.16
3	2.954	≥ 1.2	19.47	≤ 50	4.708	44.80
4	3.050	≥ 1.2	64.25	≤ 50	5.585	9.769
5	3.451	≥ 1.2	59.77	≤ 50	6.792	37.96
6	4.241	≥ 1.2	$.7488\text{x}10^{-4}$	≤ 10	8.640	$0.4083\text{x}10^{-3}$
7	4.704	≥ 1.2	6.536	≤ 10	8.887	1.481
8	4.794	≥ 1.2	22.98	≤ 10	8.906	0.6374
9	8.558	≥ 1.2	13.85	≤ 10	10.64	0.5152
10	9.277	≥ 1.2	0.2267	≤ 10	11.37	0.1674
11	10.30	≥ 1.2	8.907	≤ 10	11.67	4.509
12	12.93	$1.2 \geq \omega \geq 75$	2.220	≤ 10	16.15	9.968
13	256.8	≥ 200	$0.173\text{x}10^{-4}$	≤ 10	422.7	$0.2205\text{x}10^{-4}$
14	281.9			≤ 10	469.5	$0.2324\text{x}10^{-4}$
15	330.7			≤ 10	726.7	0
16	348.9			≤ 10	761.3	$0.1192\text{x}10^{-4}$
17	350.5			≤ 10	762.8	$0.3576\text{x}10^{-5}$
18	460.6			≤ 10	1344	0

No. of Iterations 87

Initial Mass (Scaled) 5.24

Final Mass (Scaled) 6.81

Final Design Variables:

1.439 0.8073 0.7797 1.010 0.8762 1.007 2.0 2.0 2.0 2.0 2.0 2.0

3.4 Control Analyses

Several control analyses were run to determine the effects of changes in the structure. Since Run 2 gave the same results as Run 1 and Run 3 failed to achieve a feasible design, only Runs 2 and 4 were used. The top three struts in the structure were considered to be active control elements capable of generating axial forces only.

Figure 13 shows the open-loop frequency response of the original structure from the actuators to the two LOS outputs, LOS-X and LOS-Y. Figure 14 shows the same response for frequencies less than 20 rad/sec. Note that modes 14-18 do not appear significant in the response.

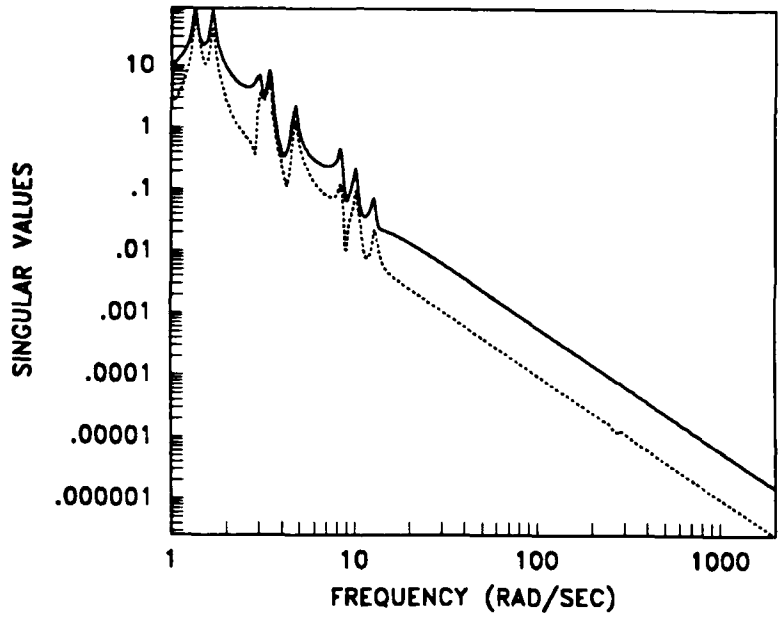

Figure 13.

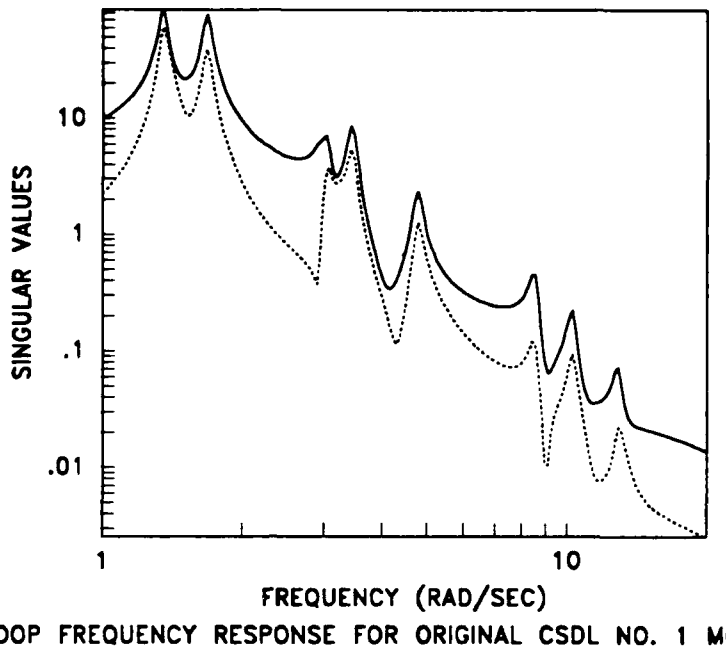

Figure 14.

Figure 15 shows the open-loop frequency response of the structure created in Run 2. The differences with the original design are not dramatic. The same holds true for the structure created in Run 4, which is shown in Figure 16.

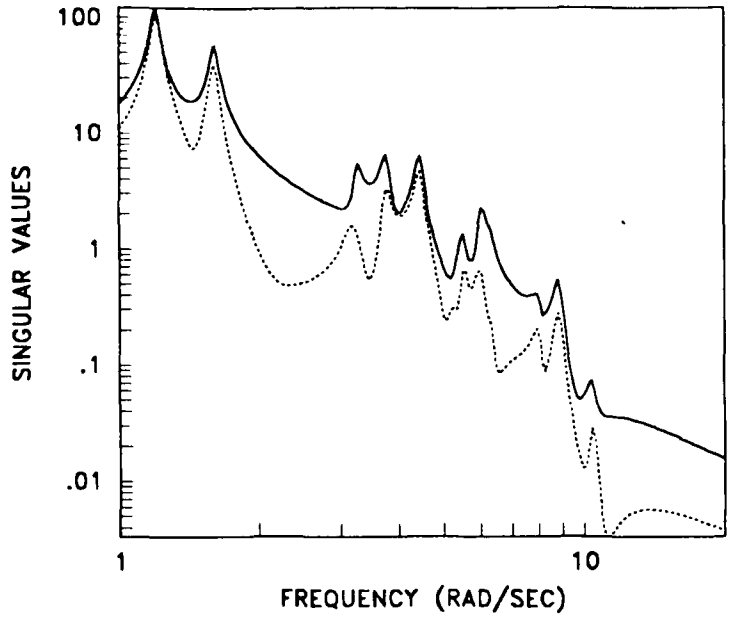

Figure 15.

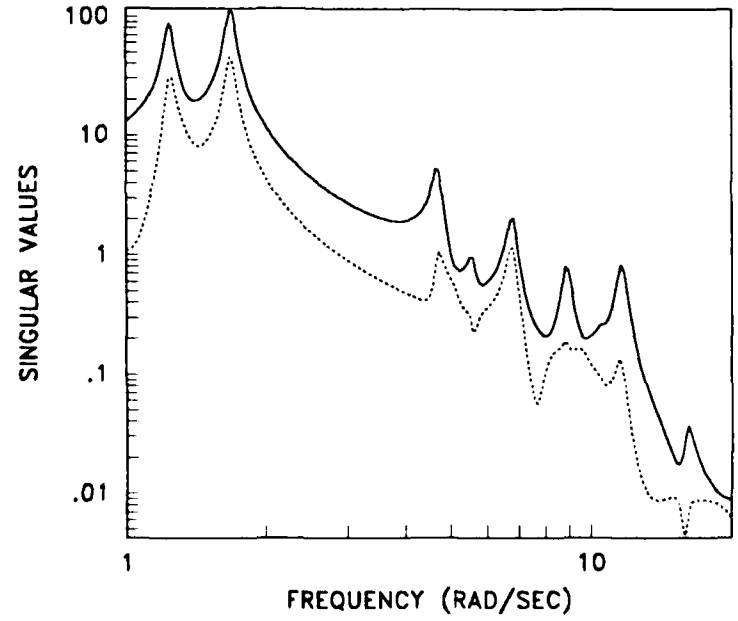

Figure 16.

To determine what effect the structural changes had on control effort and LOS performance, a series of optimal regulator designs was performed. The optimal regulator design minimized LOS and control effort. Full-state feedback was assumed, since it was not desired to raise the issue of estimation here.

Figure 17 shows the results of this analysis for the original model. LOS performance was defined to be the maximum RMS error in LOS–X and $-Y$, whereas control effort was defined to be the maximum RMS force in the three actuators.

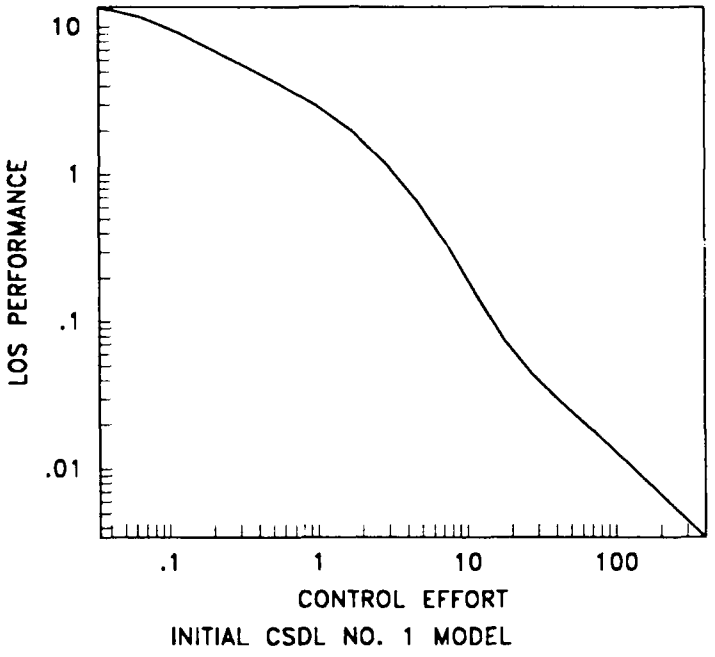

Figure 17.

Figures 18 and 19 show performance vs. effort for Runs 2 and 4. There are no significant differences with the original model. It is good to note, however, that for the Run 2 model, similar performance is achieved with a much lighter structure (3.61 vs. 5.24 mass units, scaled).

Finally, the effects of structural changes on the robustness of LQG compensator design was investigated. Three position sensors were placed on the structure, colocated with the three actuators. A Kalman filter was then designed to estimate the states of the first 13 modes. Control designs were used that had equivalent LOS performance and control effort.

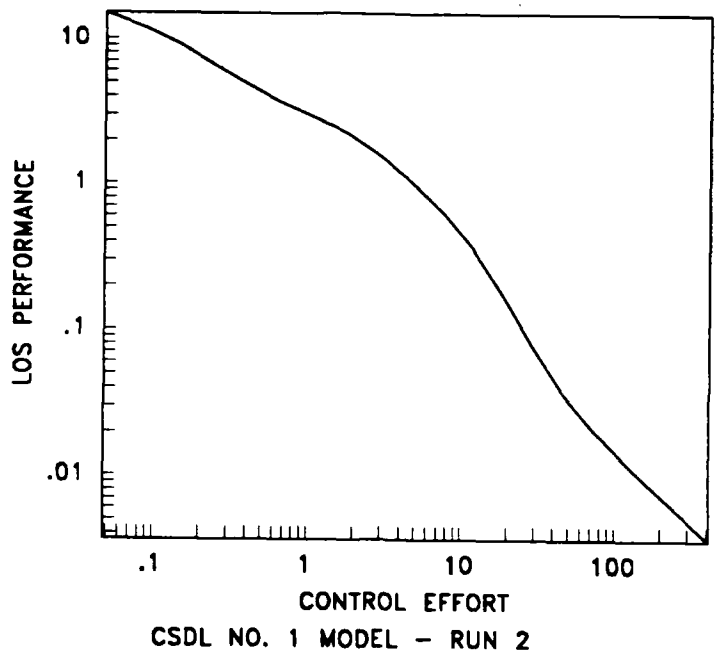

Figure 18.

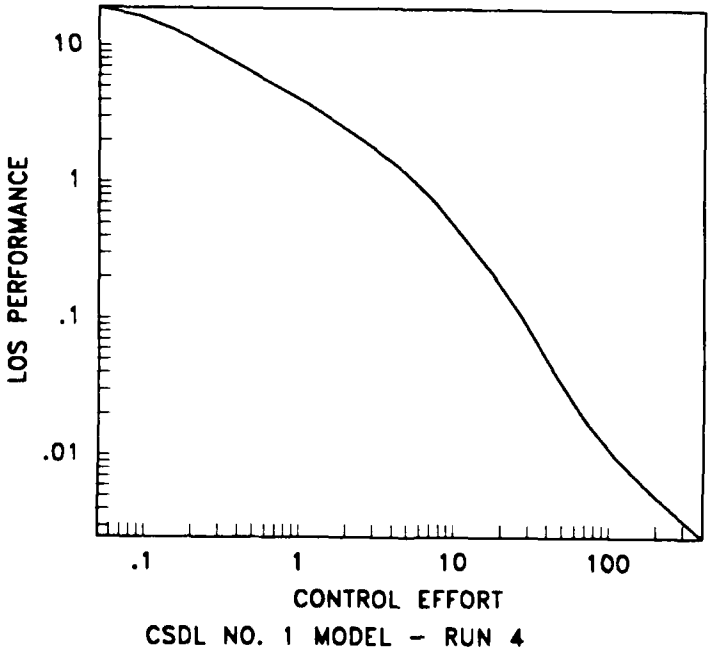

Figure 19.

Figure 20 shows the stability margin for the original design. Figures 21 and 22 show the margins for the Run 2 and Run 4 models. Again there are no significant differences.

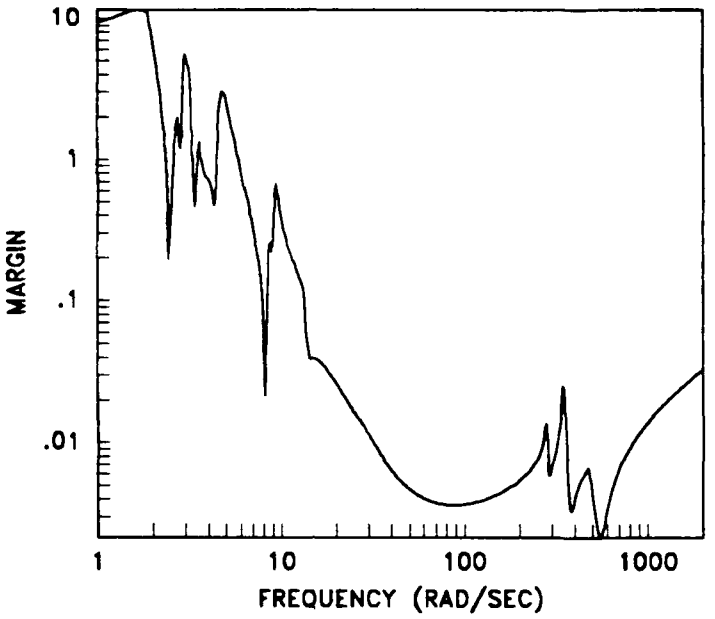

Figure 20.

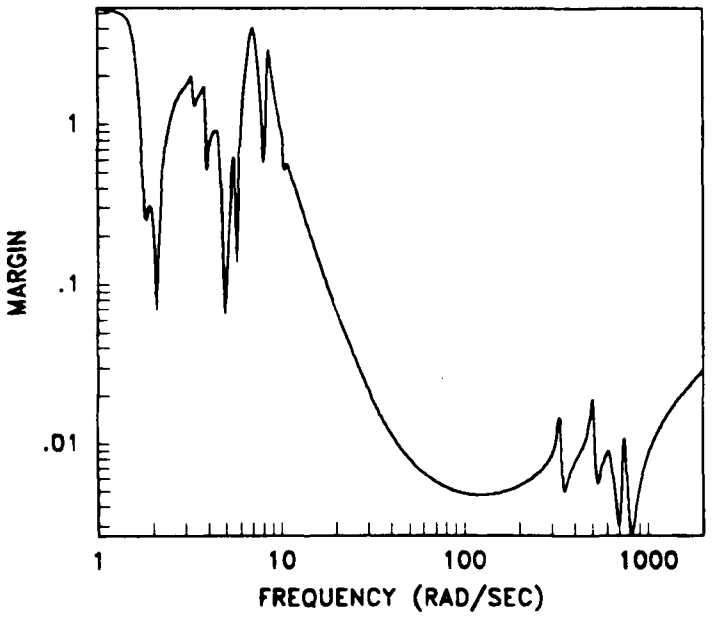

Figure 21.

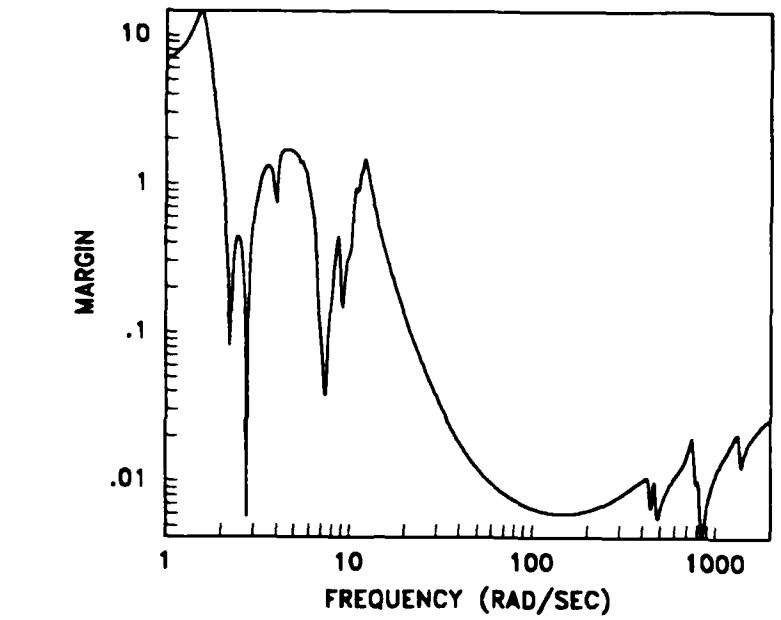
10
1
.1
.01
MARGIN
1
10
100
1000
FREQUENCY (RAD/SEC)
ADDITIVE STABILITY MARGIN FOR CSDL NO. 1 MODEL – RUN 4

Figure 22.

SECTION 4
CONCLUDING REMARKS

In the examples given above, the ability has been demonstrated to exert control, in some optimal sense, of the natural frequencies and the disturbance-rejection qualities of a structure. Although the structural models used here have only employed up to 12 design variables and 37 constraints, the techniques used have been successfully applied to much larger models in other types of optimization problems, with on the order of 100 design variables and constraints. There is therefore no reason to doubt that the problems treated in this work can be applied to models of similar complexity.

The results of the control analyses performed on CSDL Model 1 are inconclusive. Changes in the structure to reduce measures of its disturbance- rejection capabilities have not significantly altered its characteristics from a control viewpoint. CSDL Model 1 is a structure that is inherently easy to control. There is a large natural break in the frequency response, and the response rolls off almost monotonically after the first two modes. Because the structure is so simple, it does not display all of the pathologies of large space structures that the structural optimization techniques presented in this report are intended to address. Clearly, more complex test cases are required.

In terms of calculating the sensitivities that are required, everything is in place for including the other grammians in the optimization problem, so that other issues that arise in controlling flexible space structures can easily be addressed. Similarly, the extension to integrated controller and structural design with full state feedback, as presented in Reference 2, is at least conceptually a simple matter. For practical applications, however, reduced-order controllers are required, and including state estimation in the integrated design problem remains an open question. For the present, therefore, it appears advisable to continue this work along the following lines:

1. Continue the current applications with more complex models.

2. Incorporate, as appropriate, other grammians into the design problem, and evaluate suitable complex models.

3. As an intermediate step, formulate and evaluate the integrated design problem with full state feedback.

4. Investigate the formulation of the integrated design problem with state estimation included.

REFERENCES

1. Lisowski, R.J. and Hale, A.L.: Optimal Design for Single Axis Rotational Maneuvers of a Flexible Structure. AIAA Paper 84-1041, presented at the AIAA Dynamics Specialists Conference, Palm Springs, CA, May 1984.

2. Messac, A., Turner, J.D., and Soosaar, K.: An Integrated Control and Minimum Mass Structural Optimization Algorithm for Large Space Structures. Paper presented at the JPL Workshop on Identification and Control of Flexible Space Structures, San Diego, CA, June 1984.

3. Salama, M., Hamidi, M., and Demsetz, L.: Optimization of Controlled Structures. Paper presented at the JPL Workshop on Identification and Control of Flexible Space Structures, San Diego, CA, June 1984.

4. Khot, N.S., Eastep, F.E., and Venkayya, V.B.: Optimal Structural Modification to Enhance the Optimal Active Vibration Control of Large Flexible Structures. AIAA Paper 85-0627, presented at the AIAA/ASME/ASCE/AHS 26th Structures, Structural Dynamics and Materials Conference, Orlando, FL, April 1985.

5. Bodden, D.S. and Junkins, J.L.: Eigenvalue Optimization Algorithms for Structural/Controller Design Iterations. Paper presented at the 1984 American Control Conference, San Diego, CA, June 1984.

6. Lamberson, S.E. and Yang, T.Y.: Optimization Using Lattice Plate Finite Elements for Feedback Control of Space Structures. AIAA Paper 85-0592 , presented at the AIAA/ASME/ASCE/AHS 26th Structures, Structural Dynamics and Materials Conference, Orlando, FL, April 1985.

7. Haftka, R.T., Martinovic, Z.N., and Hallauer, W.L.: Enhanced Vibration Controllability by Minor Structural Modification. AIAA Journal, Vol. 23, No. 8, August 1985, pp. 1260-1266.

8. Hale, A.L.: Integrated Structural/Control Synthesis via Set- Theoretic Methods. AIAA Paper 85-0806, presented at the AIAA/ASME/ASCE/AHS 26th Structures, Structural Dynamics and Materials Conference, Orlando, FL, April 1985.

9. Gregory, C.Z.: Reduction of Large Flexible Spacecraft Models Using Internal Balancing Theory. Journal of Guidance, Control and Dynamics, Vol. 7, No. 6, November-December 1984, pp. 725-732.

10. Skelton, R.E., Hughes, P.C. and Hablani, H.: Order Reduction for Models of

Space Structures Using Modal Cost Analysis. Journal of Guidance, Control and Dynamics, Vol. 5, No. 4, July-August 1982, pp. 351-357.

11. Fox, R.L. and Kapoor, M.P.: Rates of Change of Eigenvalues and Eigenvectors. AIAA Journal, Vol. 6, No. 12, December 1968, pp. 2426-2429.

12. Cardani, C. and Mantegazza, P.: Calculation of Eigenvalue and Eigenvector Derivatives for Algebraic Flutter and Divergence Eigenproblems. AIAA Journal, Vol. 17, No. 4, April 1979, pp. 408-412.

13. Zoutendijk, G.: Methods of Feasible Directions. Elsevier Publishing Co., Amsterdam, 1960.

14. Vanderplaats, G.N.: CONMIN–A Fortran Program for Constrained Function Minimization; User's Manual. NASA TM X-62,282, August 1973; Addendum, May 1978.

15. Preston, R.B.: Pareto Optimal Vibration Damping in Large Space Structure Control. M.S. Thesis, Dept. of Aeronautics and Astronautics, Massachusetts Institute of Technology, Cambridge, MA, December 1979.

END

11-86

DTIC